JOC The Journal of Organic Chemistry

Article

pubs.acs.org/joc

Quinolone–Hydroxyquinoline Tautomerism in Quinolone 3-Esters. Preserving the 4-Oxoquinoline Structure To Retain Antimalarial Activity

Pedro Horta,[†,‡] Nihal Kuş,[§,∥] Marta Sofia C. Henriques,[⊥] José A. Paixão,[⊥] Lis Coelho,[#] Fátima Nogueira,[#] Paul M. O'Neill,[‡] Rui Fausto,*[,§] and Maria Lurdes Santos Cristiano*[,†]

[†]CCMAR and Department of Chemistry and Pharmacy, FCT, University of Algarve, P-8005-039 Faro, Portugal

[‡]Department of Chemistry, University of Liverpool, Liverpool L69 7ZD, United Kingdom

[§]CQC, Department of Chemistry, University of Coimbra, P-3004-535 Coimbra, Portugal

[∥]Department of Physics, Anadolu University, 26470 Eskişehir, Turkey

[⊥]CFisUC, Department of Physics, University of Coimbra, P-3004-516 Coimbra, Portugal

[#]CMDT and Institute of Hygiene and Tropical Medicine, New University of Lisbon, P-1349-008 Lisboa, Portugal

Supporting Information

ABSTRACT: Recent publications report *in vitro* activity of quinolone 3-esters against the bc_1 protein complex of *Plasmodium falciparum* and the parasite. Docking studies performed in silico at the yeast Q_o site established a key role for the 4-oxo and N–H groups in drug-target interactions. Thus, the possibility of 4-oxoquinoline/4-hydroxyquinoline tautomerism may impact in pharmacologic profiles and should be investigated. We describe the synthesis, structure, photochemistry, and activity against multidrug-resistant *P. falciparum* strain Dd2 of ethyl 4-oxo-7-methylquinoline-3-carboxylate (**7Me-OQE**) and ethyl 4-hydroxy-5-methylquinoline-3-carboxylate (**5Me-HQE**), obtained from diethyl 2-[((3-methylphenyl)amino)methylene]malonate. Theoretically (B3LYP/6-311++G(d,p)), **5Me-HQE** and **7Me-OQE** show clear preference for the hydroxyquinoline form. The difference between the lowest energy hydroxyquinoline and quinolone forms is 27 and 38 kJ mol^{-1}, for **5Me-HQE** and **7Me-OQE**, respectively. Calculations of aromaticity indexes show that in **5Me-HQE** both rings are aromatic, while in the corresponding oxo tautomers the nitrogen-containing ring is essentially non-aromatic. The structure of monomeric **5Me-HQE** was studied using matrix isolation coupled to FTIR spectroscopy. No traces of 4-oxoquinoline tautomers were found in the experimental IR spectra, revealing that the species present in the crystal, **5Me-HQE·HCl**, was lost HCl upon sublimation but did not tautomerize. Continuous broadband irradiation (λ > 220 nm; 130 min) of the matrix led to only partial photodecomposition of **5Me-HQE** (ca. 1/3).

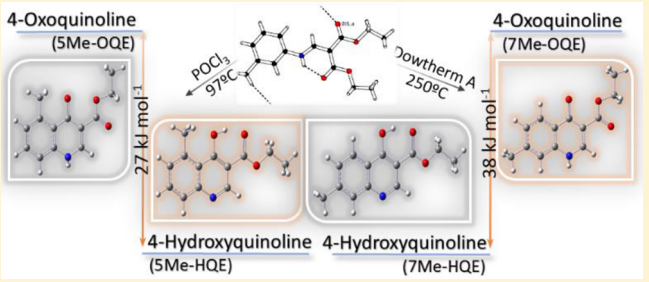

INTRODUCTION

The use of quinolones as antibacterial agents began in 1963. Following the discovery of nalidixic acid, a naphthyridone 3-acid, several quinolone derivatives with improved pharmacologic profile were synthesized. Among these, the fluoroquinolones norfloxacin, ciprofloxacin, and levofloxacin (structures are presented in Figure S1, Supporting Information) emerged as the most efficient quinolone-type antibacterial drugs and are widely used as second line antibiotics.[1,2] As shown (Figure S1), these quinolone-based antibacterial agents are *N*-alkyl-4-oxoquinoline 3-acids. The *N*-alkyl substituent was introduced to adjust pharmacologic properties.[3] Also, N-substitution hinders the possibility of quinolone-hydroxyquinoline tautomerism, restricting structural diversity of the active pharmaceutical ingredient.

The versatility of the quinolone chemotype has attracted intense research, yielding quinolones (mainly 4-oxoquinolines) with improved pharmacological properties, targeting a variety of applications, e.g., cancer,[4] hepatitis B,[5] hepatitis C,[6] HIV,[7] herpes,[8] fungal infections, immunomodulation,[9] tuberculosis,[10] or malaria.[11−14]

Malaria remains one of the most deadly infectious diseases. The growing spread of resistance by *Plasmodium falciparum* against conventional antimalarial drugs boosted the search for new chemotherapeutic solutions.[15] The approval of malarone for the treatment and prevention of multidrug-resistant malaria validated the *P. falciparum* bc_1 protein complex as target for developing new antiplasmodial drugs. The bc_1 complex is a homodimeric transmembrane protein responsible for the transfer of electrons from ubiquinol to cytochrome *c*, together with the vectorial translocation of protons across the inner

Received: September 15, 2015

DOI: 10.1021/acs.joc.5b02169
J. Org. Chem. XXXX, XXX, XXX−XXX

mitochondrial membrane. Loss of bc_1 activity leads to loss of mitochondrial function (relevant to provide intermediates for pyrimidine and ATP synthesis) as evidenced by the collapse of the transmembrane electrochemical potential, resulting in parasite death.[16,17] Figure 1 presents the structures of

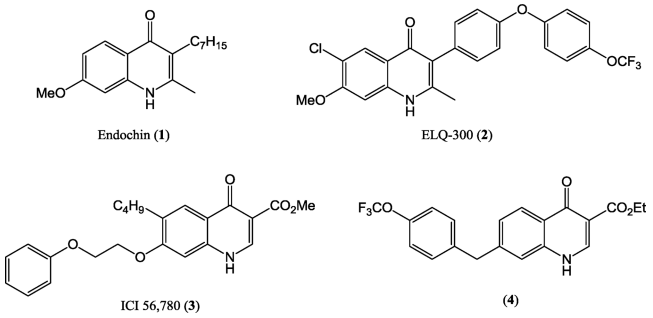

Figure 1. Structure of quinolones with relevant antiplasmodial activity.

representative quinolone-type compounds with relevant antiplasmodial activity, targeting the bc_1 protein complex of *P. falciparum*. Endochin (**1**)[18] was validated as one of the first synthetic antimalarials. It exhibits activity against avian malaria and served as model for new endochin analogues (endochin-like quinolones, ELQ) with improved therapeutic properties.[19] From these, the quinolone 3-diarylether ELQ-300 (**2**), an antimalarial preclinical candidate,[20] and the quinolone 3-ester ICI 56,780 (**3**)[21] emerged as leads.

In recent years, a range of 6- and 7-substituted quinolone 3-esters have been prepared and tested *in vitro* against *P. falciparum* malaria parasites. Interestingly, some 7-substituted derivatives (**4**) expressed activity at low nanomolar concentrations.[14] Docking studies performed *in silico* at the yeast Q_o site of the bc_1 protein complex of *P. falciparum* suggested a key role for residues His182 and Glu272 (in the target ISP) in the recognition of high-potency inhibitors. The same studies also indicated that the 4-oxoquinoline moiety is oriented so as to enable formation of an H-bond between the quinolone carbonyl and a protonated imidazole N atom of His181, while a second H-bond (water mediated) is predicted between the carboxyl group of the cytochrome *b* residue Glu272 and the quinolone N−H. Thus, both the 4-oxo substituent and the N−H group appear to be important to the inhibitory activity of quinolone 3-esters toward *P. falciparum* bc_1 protein complex.[14] It is noteworthy that, unlike for the antibacterial fluoroquinolone drugs (see Figure S1), compounds **1**−**4** (Figure 1) bear these structural characteristics.

Although some 7-substituted quinolone 3-esters appear highly promising as drug leads, the compounds present liabilities, such as poor aqueous solubility and low oral bioavailability. Preliminary results from structure−activity relationship (SAR) studies indicated that optimization could be achieved by tuning the nature of substituent at position 7.[14] Additionally, considering that the information from docking studies *in silico* establishes a relevant role for the 4-oxo and N−H groups in drug−target interactions, the possibility of tautomerism between 4-oxoquinoline and 4-hydroxyquinoline forms (**5**, **6**; Figure 2) should not be neglected. Tautomerization will translate in alteration of chemical and physical properties, with possible implications in pharmacokinetic and pharmacodynamic profiles.

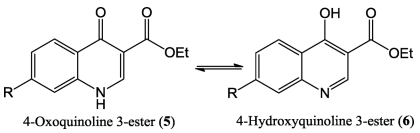

Figure 2. 4-Oxo/4-hydroxy tautomeric equilibrium in 7-substituted quinoline 3-esters.

Thus, we envisaged investigating the tautomer and conformer preferences in quinolone 3-esters, using ethyl 4-oxo-7-methylquinoline-3-carboxylate (Figure 2; **5**; R = CH_3) as our model compound. For simplicity, we refer to this compound as 7-methyl-oxoquinoline-ester (**7Me-OQE**).

We describe herein the synthesis and structure of the quinolone 3-ester **7Me-OQE**. This compound was obtained by thermal cyclization of diethyl 2-[((3-methylphenyl)amino) methylene]malonate **9** in dowtherm A at 250 °C (see Scheme 1, route c) and isolated as sole product. The corresponding 4-hydroxyquinoline tautomer (Figure 2; **6**; R = CH_3) was not observed. Surprisingly, cyclization of compound **9** mediated by $POCl_3$, at 100 °C, led to a mixture of an amorphous powder and crystals. Analysis of one of these crystals by X-ray crystallography revealed the presence of the hydrochloride salt of one hydroxyquinoline 3-ester isomer, ethyl 4-hydroxy-5-methylquinoline-3-carboxylate **10** (see Scheme 1, route d; HCl is formed as byproduct from $POCl_3$-mediated cyclization). For simplicity, we refer to 4-hydroxyquinoline **10** as 5-methyl-hydroxyquinoline-ester (**5Me-HQE**) and to its hydrochloride salt as **5Me-HQE·HCl**. The crystal structure of **5Me-HQE·HCl** is described. The structure of monomeric **5Me-HQE** was investigated, using matrix isolation coupled to FTIR spectroscopy (upon sublimation of **5Me-HQE·HCl**, HCl is evolved and sole the free base, **5Me-HQE**, is isolated in the argon matrix) and theoretical calculations (B3LYP/6-311++G(d,p)). A detailed analysis of conformational and tautomeric preferences for **5Me-HQE** is provided, and the possibility of quinolone-hydroxyquinoline equilibria is evaluated. The conformational and tautomeric preferences for monomeric 4-oxoquinoline **7Me-OQE** were also theoretically investigated, at the same level of theory.

The photostability of **5Me-HQE** was assessed through an investigation of its UV-induced matrix photochemistry. The antiplasmodial activity of 4-oxoquinoline **7Me-OQE** and 4-hydroxyquinoline **5Me-HQE** against the chloroquine and mefloquine-resistant *P. falciparum* strain Dd2[22] was evaluated.

RESULTS AND DISCUSSION

Synthesis. Quinolone 3-esters may be prepared from an α,β-unsaturated ester derivative of aniline (usually a malonate derivative) through a thermally driven intramolecular cyclization. This approach, known as the Gould−Jacobs methodology,[23] presents limitations, mostly related to the high temperature (above 225 °C) required for reaction. Cyclization was found to be concentration dependent, and the product may undergo thermal degradation.[8] Because most quinolones exhibit low solubility, leading to difficulties in extraction and purification, an alternative methodology for cyclization, using phosphoryl chloride, was proposed. This approach involves cyclization of the enamine and chlorination at the 4-position, in one pot.[24] It is anticipated that the 4-chloroquinoline produced will be more easily isolated and may be subsequently converted into the final quinolone. Also, the 4-chroroquinoline may be

DOI: 10.1021/acs.joc.5b02169
J. Org. Chem. XXXX, XXX, XXX−XXX

Scheme 1. Synthetic Approach to Ethyl 4-oxo-7-Methylquinoline-3-carboxylate, 7Me-OQE (5, R = CH_3), and to Ethyl 4-Hydroxy-5-methylquinoline-3-carboxylate, 5Me-HQE (10)[a]

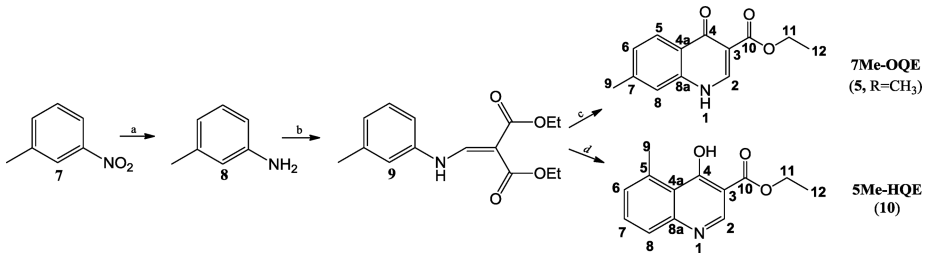

[a]Conditions: (a) NH_4Cl, Fe(II), MeOH:H_2O (1:1), 60 °C, 4 h; (b) 100 °C, o.n.; (c) Dowtherm A, 250 °C, 3 h; (d) $POCl_3$, 97 °C, o.n.

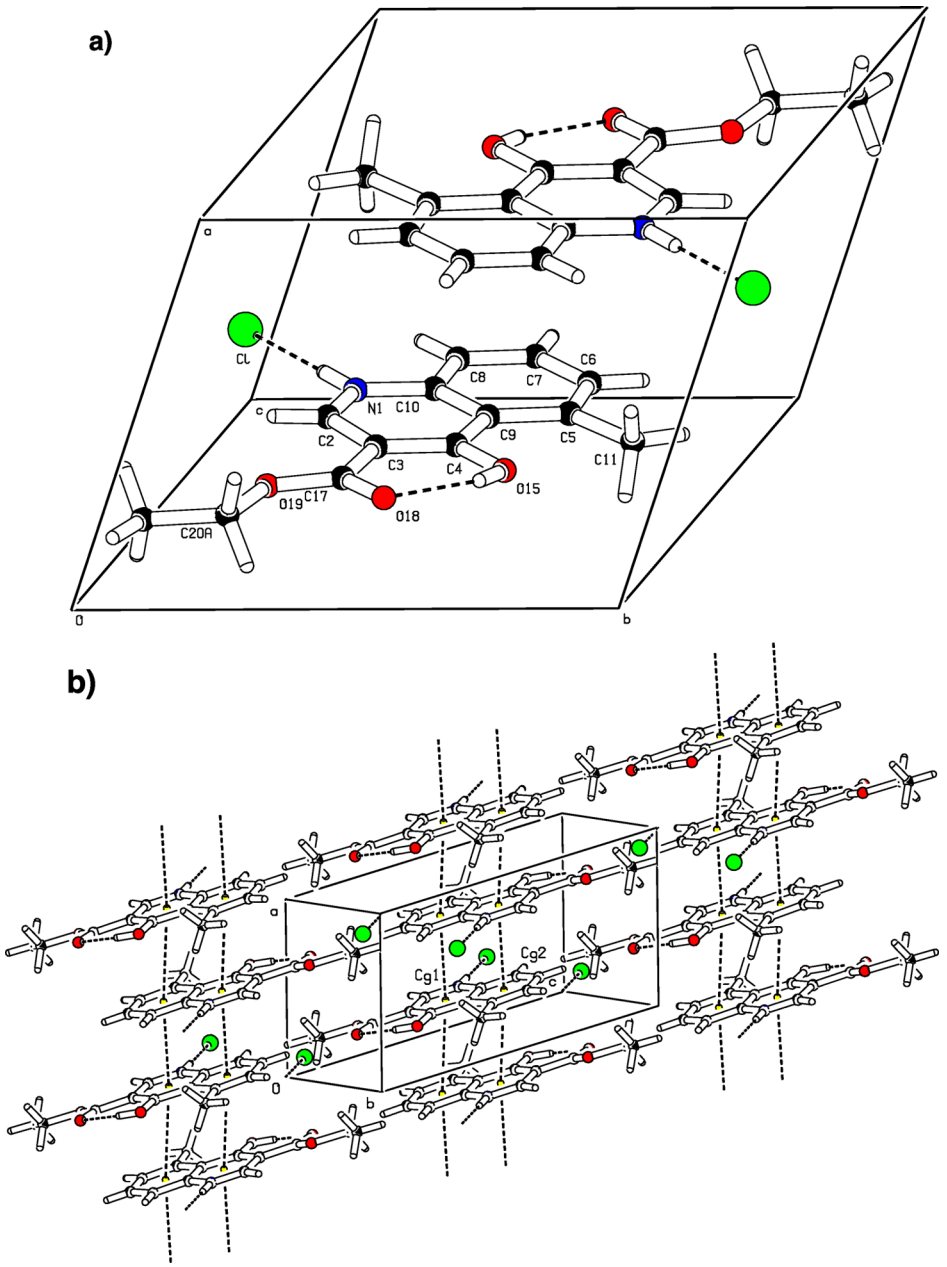

Figure 3. Crystal structure of ethyl 4-hydroxy-5-methyl quinolinium chloride 3-carboxylate (chloride salt of **10**), showing (a) the intramolecular H-bonding pattern; (b) molecular stacking and interactions between π electron clouds of aromatic rings. The ethyl group is disordered over two alternate positions; for clarity, only the atoms of the position of larger occupancy are shown in the figure. An ORTEPII plot of the **5Me-HQE·HCl** molecule is provided in Figure S11.

DOI: 10.1021/acs.joc.5b02169
J. Org. Chem. XXXX, XXX, XXX−XXX

used as an intermediate for the synthesis of quinoline derivatives.[25]

The synthetic approach that led to quinolone **7Me-OQE** and of hydroxyquinoline **5Me-HQE** (or corresponding salt, **5Me-HQE·HCl**) was performed as depicted in Scheme 1. Both compounds were prepared from 3-nitrotoluene **7**, in three steps. 3-Nitrotoluene **7** was initially reduced to 3-methylaniline **8**, which was converted into the diethylmalonate derivative **9**. Both steps (a, b; Scheme 1) were optimized and afforded high yields of the isolated products.

The crystal structure of compound **9** was determined by X-ray crystallography (Figure S4). Atomic coordinates, bond lengths, valence and dihedral angles, and other crystallographic data were deposited at the Cambridge Crystallographic Data Centre, with the reference CCDC 1039617 (see Figure S4 for crystal structure and interpretation of crystallographic data). Bond lengths and valence angles of the diethyl 2-[((3-methylphenyl)amino) methylene]malonate molecule **9** are within the expected values.

As shown in Scheme 1, two methods were followed for the preparation of quinoline derivatives from **9**. Thermal cyclization of **9** in Dowtherm A at 250 °C (Gould−Jacobs methodology) afforded quinolone **7Me-OQE** (**5**; R = CH_3, route c). However, cyclization of **9** mediated by $POCl_3$, at 100 °C, led to formation of hydroxyquinoline **5Me-HQE** (**10**; route d). According to the literature[24] this strategy should afford 4-chloroquinoline, but, in our case, a mixture of hydroxyquinoline (**10**, **5Me-HQE**) and its hydrochloride salt (**5Me-HQE·HCl**) was recovered.

In the thermally driven cyclization it is proposed that the phenyl ring acts as nucleophile, attacking the carbon of the ester carbonyl group.[23] It is worth noticing that routes c and d afforded quinolines with different patterns of aromatic substitution, resulting from cyclization on both ortho carbons of the aniline derivative **9**.

7Me-OQE and **5Me-HQE** are easily distinguished by ^{1}H NMR and ^{13}C NMR spectroscopy (see Scheme 1 for atom numbering in 4-oxoquinoline and 4-hydroxyquinoline structures). Important ^{1}H NMR signals (in d_6-DMSO) for identification of quinolone **7Me-OQE** are those due to resonances of H1 (N−H; bs, δ = 12.17 ppm) and H8 (Ar−H; s, δ = 7.38 ppm). Relevant ^{13}C NMR signals (in d_6-DMSO) for **7Me-OQE** are those due to resonance of the carbonyl carbon of the oxoquinoline system, C4, and to the carbonyl carbon of the ester group, C10 (C4 δ = 176.0 ppm; C10 δ = 165.0 ppm). These signals confirm formation of 4-oxoquinoline **7Me-OQE** from step c (Scheme 1). Figures S5 and S6 present predicted ^{1}H NMR and ^{13}C NMR chemical shifts (ppm) and the corresponding experimental ^{1}H NMR and ^{13}C NMR spectra for **7Me-OQE** in d_6-DMSO.

Analysis of the product isolated from step d (Scheme 1) revealed the presence of 4-hydroxyquinoline **5Me-HQE** (**10**, Scheme 1). In this case, cyclization led to a 4-hydroxyquinoline 3-ester methyl-substituted at position 5.

The ^{1}H NMR spectra of crystalline hydroxyquinoline **5Me-HQE** (see Figures S8 and S10), in d_6-DMSO and in *d*-chloroform, show the absence of a signal corresponding to the resonance of the proton from the N−H bond. Despite presenting coincident splitting patterns that are compatible with the hydroxyquinoline form, the ^{1}H-chemical shifts are different in d_6-DMSO and in *d*-chloroform, the difference being more pronounced for signals corresponding to H2 and H8. The proton resonances for **5Me-HQE** in *d*-chloroform appear downfield (H2, Ar−H, d, δ = 9.26 ppm; H8, Ar−H, s, δ = 8.51 ppm), compared to the corresponding resonances in d_6-DMSO (H2, Ar−H, d, δ = 8.38 ppm; H8, Ar−H, s, δ = 7.44 ppm). This difference is ascribed to the dissociation of the salt in d_6-DMSO, with loss of HCl and release of the free base. The ^{1}H NMR spectrum of **7Me-OQE** was also measured in *d*-chloroform (see Figure S7). For this compound, there was no evidence in the spectra of significant differences in the ^{1}H-chemical shifts in d_6-DMSO and in *d*-chloroform. So, it appears reasonable to deduce that the differences in chemical shifts observed for **5Me-HQE** in both solvents were due to loss of HCl from the salt with formation of the free base, induced by the more polar media.

The ^{13}C NMR spectrum of the crystalline **5Me-HQE** in d_6-DMSO (see Figure S9) shows characteristic signals for compound **10**, corresponding to resonances of C4 (see Scheme 1 for atom numbering), at δ = 171.1 ppm (predicted at δ = 184.2 ppm for the quinolone tautomer), C8 and C8a, at δ = 127.9 and 161.3 ppm (predicted at δ = 114.5 and 141.4 ppm, respectively, for the quinolone tautomer), demonstrating the sole presence of the 4-hydroxyquinoline tautomer (**5Me-HQE**) in solution. Figures S8 and S9 present the chemical shifts (ppm) predicted for ^{1}H- and ^{13}C NMR spectra of **5Me-HQE** and the corresponding experimental spectra, in d_6-DMSO.The data obtained from elemental analysis of the powder obtained from step d (Scheme 1) are compatible to calculated values for the free base, **5Me-HQE**.

Crystal Structure of 5Me-HQE·HCl. The crystal structure of the hydrochloride salt of **5Me-HQE** is presented in Figure 3. Atomic coordinates, bond lengths, valence angles, dihedral angles, and other crystallographic data were deposited at the Cambridge Crystallographic Data Centre, with the reference CCDC 1039599.

Each unit cell contains two anion−cation pairs, related by an inversion center. Bond lengths and valence angles are within the expected values. Two strong H-bonds are evidenced, one between the amine group and the halide ion (N1···Cl: 2.955(2) Å), the other between the hydroxyl substituent at C4 and the oxygen of the ester carbonyl group (O15···O18:2.570 (3) Å). In addition, a short contact distance C−H···Cl of 3.645(4) Å involving the C6 atom can be spotted in the structure. The major intermolecular interactions stabilizing the crystal structure are probably weak dispersion forces (π−π type interactions) between the π electron clouds of the aromatic carbocyclic rings. The stacking of the molecules is such that the electron clouds of each N-substituted ring in one layer interact with those of two methyl-substituted phenyl rings in adjacent layers and vice versa, as depicted in Figure 3b. The distances between the centers of gravity of the rings (Cg1: N1−C2−C3−C4−C9−C10; Cg2: C5−C6−C7−C8−C10−C9) in these four intermolecular interactions are typical for parallel interaction between two aromatic rings (Cg1−Cg2^i: 3.629(2); Cg1−Cg2^{ii}: 3.625(2); Cg1−Cg2^i: 3.630(2); Cg1−Cg2^{ii}: 3.624(2); i = $-x$,1 − y,1 − z; ii = 1 − x,1 − y,1 − z).

ATR-FTIR Experiments. **7Me-OQE** and **5Me-HQE** may also be distinguished by FTIR spectroscopy. The ATR spectra of crystalline samples of the two compounds and the proposed band assignments are shown in Figure S12 and Tables S2 and S3. As it could have been anticipated, the two spectra do not differ much, except in the characteristic regions of the OH group, present in **5Me-HQE** and absent in **7Me-OQE**, and for the carbonyl stretching mode of the quinolone carbonyl group of this latter compound, absent in the first. Specifically, (i) the spectrum of **5Me-HQE** is by far more complex in the high-

DOI: 10.1021/acs.joc.5b02169
J. Org. Chem. XXXX, XXX, XXX−XXX

frequency region, where bands due to the νOH mode are observed (this profile is complicated by the coupling of this mode with low-frequency intermolecular modes and involvement of the OH group in the intramolecular H-bond with the ester group), (ii) a band is observed at 1426 cm^{-1} in the spectrum of **5Me-HQE**, which has no counterpart in the spectrum of **7Me-OQE**, ascribable to the δCOH bending, (iii) a shoulder due to the stretching mode of the quinolone carbonyl group of **7Me-OQE** is observed at 1724 cm^{-1}, at a position where no absorption is observed in the spectrum of **5Me-HQE**. The τOH mode of **5Me-HQE** was tentatively assigned to the band at 861 cm^{-1} in the spectrum of **5Me-HQE**, but the complexity of the two spectra in this frequency range precludes a definitive assignment of this vibration. On the other hand, since the spectrum of **5Me-HQE** corresponds to that of the HCl salt of the compound, the quinolinic N is protonated in both compounds, and the vibrations of this moiety are observed at similar frequencies (see Tables S2 and S3).

The crystalline **5Me-HQE·HCl** was washed with an aqueous solution of sodium bicarbonate. Analysis of the resulting compound revealed the presence of the corresponding keto form, **5Me-OQE** (**11**), resulting from tautomerization in basic media. The ATR-IR spectrum of **5Me-OQE** (**11**) is similar to that of the **7Me-OQE** (quinolone form) in the high-frequency region. However, as described in detail below, matrix isolation studies on this sample show that during sublimation **5Me-OQE** converts extensively to the most stable in the gas phase quinoline form (**5Me-HQE**).

Molecular Structure of Tautomers of 5Me-HQE. The tautomerism involving the 4-quinolone (oxoquinoline)/4-hydroxyquinoline system may be compared to the equilibrium between 4-pyridones (oxo form) and 4-hydroxypyridines.[26] For this system, it was found that the keto form is more stable in the crystal and in the liquid phase or in solution, while the enol form predominates in the vapor phase.[26] For the compound in study we may consider the equilibrium between the 4-hydroxyquinoline and 4-quinolone (oxoquinoline) forms shown in Figure 4: ethyl 4-hydroxy-5-methylquinoline-3-carboxylate (**5Me-HQE**; **10**), ethyl 4-oxo-5-methylquinoline-3-carboxylate (**5Me-OQE**; **11**), and 3-[ethoxy(hydroxy)-methylidene]-4-oxo-5-methylquinoline (**12**). For simplicity, we refer to **11** as **5Me-OQE** (5-methyl-oxoquinoline-ester) and to **12** as **5Me-OQHE** (5-methyl-oxoquinoline-hydroxy ester).

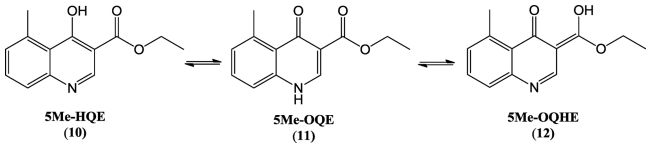

Figure 4. Possible tautomers of ethyl **5Me-HQE** considered in this work.

As shown above, analysis by X-ray crystallography demonstrated the presence in the crystal of the hydrochloride salt of the 4-hydroxyquinoline form, **5Me-HQE·HCl**. It was also demonstrated by NMR spectroscopy that the 4-hydroxyquinoline **5Me-HQE** form exists solely in solution. We also observed that the quinolone form, **5Me-OQE**, may be prepared from alkaline washing of the salt, **5Me-HQE·HCl**.

To assess the relative importance of the different tautomers of the compound as isolated species (or in the gas phase), we investigated the structure of monomeric **5Me-HQE**, using the matrix isolation technique coupled to FTIR spectroscopy and theoretical methods (DFT/B3LYP/6-311++G(d,p)). The 7Me-substituted analogue was also investigated theoretically, at the same level of theory, for comparison.

Theoretical Calculations. Investigation of the potential energy surface of the 4-hydroxyquinoline tautomer **5Me-HQE**, at the B3LYP/6-311++G(d,p) level of computation, yielded 8 nonequivalent-by-symmetry conformers, graphically depicted in Figure 5. Relative energies of these conformers are given in Table 1. As shown, two of the conformers (**I** and **II**) have much lower energy than all the other forms. Forms **I** and **II** shall represent ca. 78% and 22% of the total population in the gas phase equilibrium at room temperature, according to Boltzmann distribution. The higher-energy forms are experimentally irrelevant under these conditions.

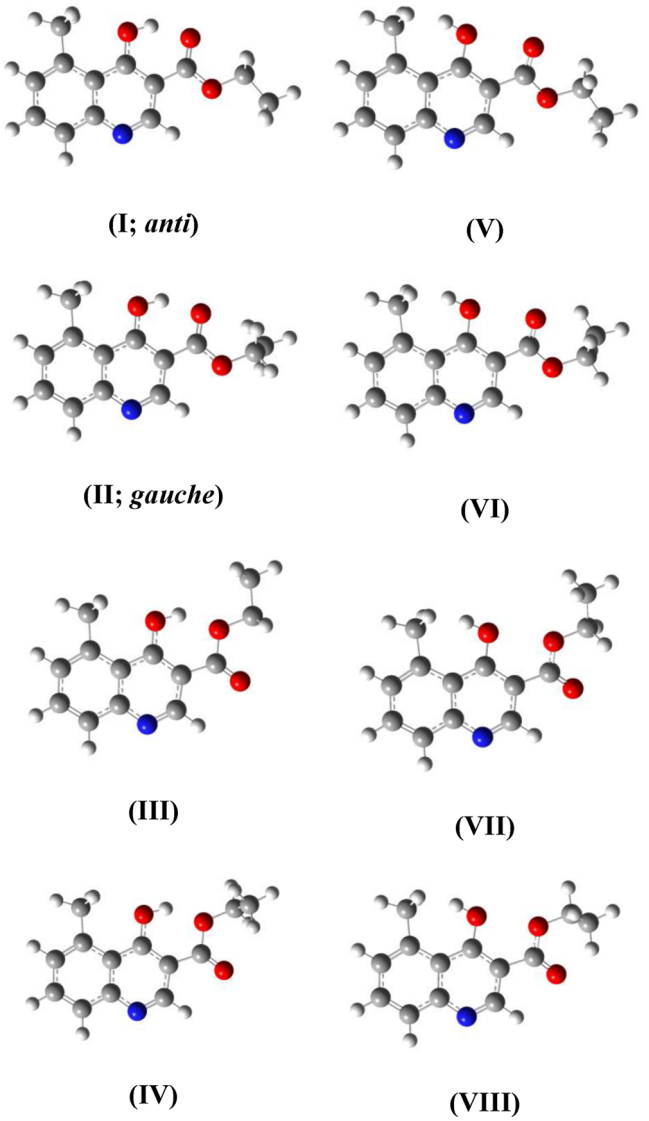

Figure 5. Conformers of the 4-hydroxyquinoline form of **5Me-HQE**.

It is clear from the relative energies of the various conformers of **5Me-HQE**, shown in Table 1, and corresponding structures, shown in Figure 5, that the considerably lower energy of forms

DOI: 10.1021/acs.joc.5b02169
J. Org. Chem. XXXX, XXX, XXX−XXX

Table 1. Relative Energies (ΔE, kJ mol^{-1}) and Relative Gibbs Energies ($\Delta G_{298.15}$, kJ mol^{-1}) of the Relevant Conformers of the Tautomeric forms of 5Me-HQE

	ΔE	$\Delta G_{298.15}$
5Me-HQE I (anti)	0.0	0.0
II (gauche)	1.9	4.8
III	17.3	17.7
IV	18.3	20.5
V	61.3	57.5
VI	63.0	59.9
VII	60.6	57.1
VIII	62.3	59.8
5Me-OQE I	26.6	23.8
II	28.7	27.5
III	34.4	31.3
IV	35.4	33.3
5Me-OQHE I	157.8	151.8
II	160.2	154.3

I and **II** (**II** is higher in energy than **I** by only 1.9 kJ mol^{-1}; 2.6 kJ mol^{-1} if zero-point corrections to energy are included) can be correlated with the presence in these forms of the O−H···O$_{(carbonyl)}$ stabilizing intramolecular H-bond interaction. Forms **III** and **IV** are of higher energies than the most stable forms by ∼18 kJ mol^{-1}, while all the remaining forms have relative energies higher than 60 kJ mol^{-1}. The intermediate relative energies of forms **III** and **IV** can be ascribed to the presence in these forms of the O−H···O$_{(ester)}$ stabilizing intramolecular H-bond interaction. This type of H-bond is well-known to be weaker than the O−H···O$_{(carbonyl)}$ one, since the carbonyl oxygen has a better ability to act as H-bond acceptor.[27,28] In forms **V** to **VIII**, no intramolecular H-bonds exist, and repulsive interactions between the OH and ester substituents dominate, thus justifying their much higher energies.

The calculated potential energy profile for internal rotation about the COCC dihedral, interconverting conformers **I** and **II** is depicted in Figure 6. The two conformers are separated by a

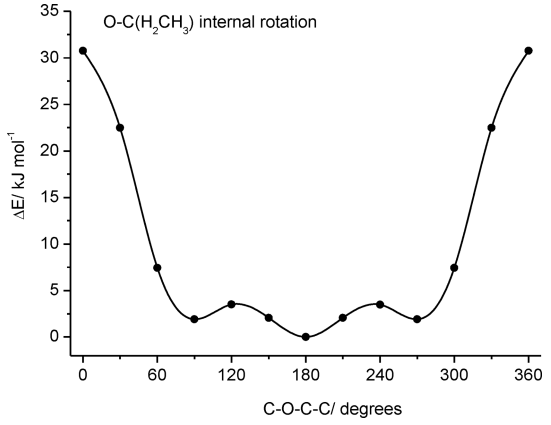

Figure 6. B3LYP/6-311++G(d,p) calculated relaxed potential energy profile for interconversion between conformers **I** and **II** of **5Me-HQE**.

small energy barrier (3.5 kJ mol^{-1} in the **I** → **II** direction; 1.6 kJ mol^{-1} in the reverse direction), the transition state (with two symmetry equivalent forms) having the COCC dihedral equal to ∼126°. Direct interconversion between the two symmetry-equivalent gauche (II) forms implies crossing a large energy barrier (∼30 kJ mol^{-1}) corresponding to the highly sterically hindered transition state with COCC dihedral equal to 0°.

Calculations at the same level of theory were also performed on the oxoquinoline tautomers of **5Me-HQE** represented in Figure 4, specifically those implying migration of H from the hydroxyl to the ring nitrogen (**5Me-OQE**, **11**) or to the ester carbonyl oxygen atom (**5Me-OQHE**, **12**).

The calculated conformers of **5Me-OQE** and **5Me-OQHE** are represented in Figures 7 and 8. For tautomer **11**, the

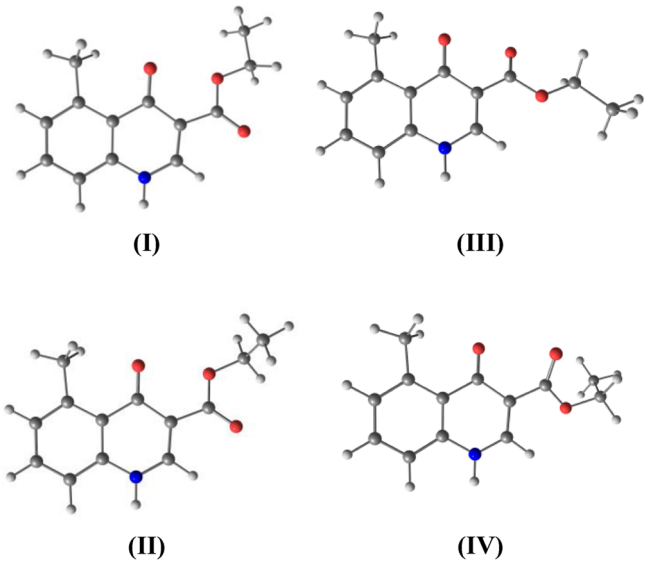

Figure 7. Selected (lowest energy) forms of the **5Me-OQE** tautomer.

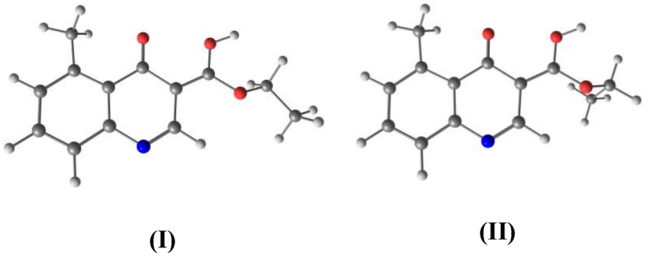

Figure 8. Selected (lowest energy) forms of the **5Me-OQHE** tautomer. The two structures of **5Me-OQHE** similar to I and II but with the OH group pointing to the carbonyl ring oxygen atom were found to converge barrierlessly to structures **5Me-HQE I** and **II**, respectively.

calculations (Table 1) show that the most stable conformer (**5Me-OQE I**) is higher in energy than the most stable conformer of the hydroxyquinoline tautomer (**5Me-HQE I**) by 27 kJ mol^{-1}. For tautomer **12**, the two lowest energy conformers have larger energies than **5Me-HQE I** by more than 155 kJ mol^{-1} (Table 1).

The relative stability of the hydroxyquinoline and oxoquinoline tautomers of the 7-Me substituted quinoline (**5** and **6** in Figure 2; R = CH$_3$) was also evaluated, leading to the same conclusions as for compound **10**. In particular, the hydroxyquinoline form is more stable in the gas phase than the oxo forms (the calculated energy difference between the most stable conformers of **7Me-OQE** and **7Me-HQE** is ∼38.0 kJ mol^{-1}). Like **5Me-HQE**, the **7Me-HQE** hydroxyquinoline tautomer has also two low-energy conformers of nearly the same energy (anti and gauche in the conformation of the ethyl ester group and

DOI: 10.1021/acs.joc.5b02169
J. Org. Chem. XXXX, XXX, XXX−XXX

exhibiting an OH···O=C intramolecular H-bond) that are similar to the two most stable forms of **5Me-HQE**). This allows to conclude that, at least from the qualitative point of view, both the tautomeric and conformational patterns in the studied molecules are not significantly affected by the position of the methyl substituent on the benzenic ring of the quinoline moiety.

In order to get some clues on reasons for the calculated relative energies of **5Me-HQE** and its two investigated tautomers (**5Me-OQE**, **11** and **5Me-OQHE**, **12**) we have estimated the aromaticity of the two rings in the molecules, using two well-known aromaticity indexes, the harmonic oscillator measure of aromaticity (HOMA index), defined by Kruszewski and Krygowsky[29] and then generalized by Krygowsky,[30] and the Bird index.[31]

The HOMA value can be obtained making use of eq 1:

$$\mathrm{HOMA} = 1 - \frac{\alpha}{n}\sum_{i=1}^{n}(R_{\mathrm{opt}} - R_i)^2 \quad (1)$$

where n is the total number of the atoms considered, R_i a bond length, and α and R_{opt} are precalculated constants given in original paper[26] for each type of atom pair (257.7 and 1.388 for C−C and 93.52 and 1.334 for C−N, respectively). If HOMA = 1, the length of each bond is identical to optimal value R_{opt}, and thus the ring is fully aromatic. If HOMA = 0, the ring is completely non-aromatic. If HOMA assumes a significantly negative value, then the ring shows anti-aromaticity character. Despite its simplicity, this index has been found to be one of the most effective structural indicators of aromaticity and a good measure of π-electron delocalization.

The Bird index is another geometry-based quantity aimed at measuring aromaticity. It can be obtained through eqs 2 and 3:

$$B_{\mathrm{I}} = 100[1 - (V/V_k)] \quad (2)$$

$$V = \frac{100}{\bar{N}}\sqrt{\frac{\sum_i (N_{i,j} - \bar{N})^2}{n}} \qquad N_{i,j} = \frac{a}{R_{i,j}} - b \quad (3)$$

In eq 3, i cycles all of the bonds in the ring, j denotes the atom next to atom i, n is the total number of the bonds considered, N denotes Gordy bond order, N is the average value of the n values, and $R_{i,j}$ is a bond length. Parameters a and b are predefined for each type of bond, being 6.8 and 1.71 for C−C and 6.48 and 2.00 for C−N, respectively. V_K is a predetermined reference value for V; for six-membered rings, this value is 33.2. The closer the Bird index is to 100, the stronger the aromaticity is.

The calculated HOMA and B_{I} indexes for **5Me-HQE**, **5Me-OQE**, and **5Me-OQHE** tautomers, using the B3LYP/6-311++G(d,p) calculated bond lengths, are given in Table 2.

Table 2. Calculated Aromaticity Indexes (HOMA and Bird) for 5Me-HQE Tautomers (10−12)

	tautomer		
	10	**11**	**12**
HOMA			
C_5N-ring	0.73	0.04	−0.07
C_6-ring	0.76	0.90	0.89
B_{I}			
C_5N-ring	78.7	57.3	60.2
C_6-ring	80.0	88.3	88.1

Qualitatively, the two indexes agree with each other: In **5Me-HQE**, both rings are aromatic, with the heteroaromatic ring being only slightly less aromatic than the benzenic ring; however, in both **5Me-OQE** and **5Me-OQHE**, the nitrogen-containing ring is essentially non-aromatic, the benzenic ring being in these cases somewhat more aromatic than in **5Me-HQE**. The reduced aromaticity of the heterocyclic ring in both **5Me-OQE** and **5Me-OQHE** compared to **5Me-HQE** can then also be considered a relevant factor rendering these species more energetic than **5Me-HQE**.

Matrix-Isolation FTIR and Photochemical Experiments. From the theoretical results presented in the previous section, it is likely to expect prevalence of **5Me-HQE** (forms **I** and **II**), in the gas phase. However, taking into account the low-energy barrier for conversion of conformer **II** into the most stable conformer **I** (only 1.6 kJ mol^{-1}), we can expect that at least partial conversion of **II** into **I** takes place during preparation of the low temperature matrices prepared from deposition of the vapor of the compound onto the cold (15 K) IR transparent CsI optical substrate of the cryostat (conformational cooling).[32] Since the gas-phase population of **II** is already small (~22%, according to the performed calculations), and the predicted IR spectra for the two conformers are quite similar (see the B3LYP/6-311++G(d,p) calculated IR spectra for the two conformers in Figure S13), presence of conformer **II** in the studied argon matrix could not be safely established. In fact, the IR spectrum of **5Me-HQE** isolated in solid argon can be fairly well reproduced by the calculated spectrum of conformer **I** alone (Figure 9).

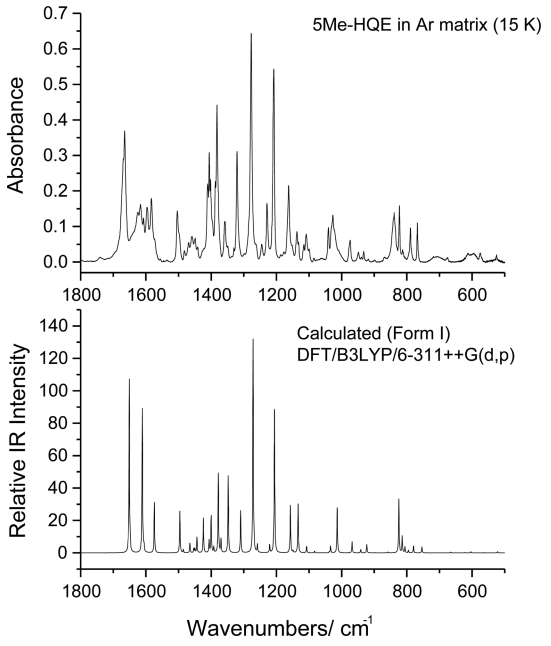

Figure 9. IR spectrum of the as-deposited argon matrix of **5Me-HQE** (top) and calculated spectrum for conformer **I** (bottom).

Annealing of the matrix up to about 40 K led to small, but perceptible changes in the relative band intensities. These might be taken as indication that conformer **II** could have partially survived to matrix deposition and is being converted into **I** upon the annealing. However, such intensity changes can also be due to matrix-site conversions or change of relative intrinsic intensities of the different bands with temperature,

DOI: 10.1021/acs.joc.5b02169
J. Org. Chem. XXXX, XXX, XXX−XXX

Table 3. Observed IR Frequencies for 5Me-HQE in Argon Matrix (15 K) and B3LYP/6-311++G(d,p) Calculated Frequencies and IR Intensities for Conformers I and II[a]

Observed (Ar matrix; 15 K)	Conformer **I**		Conformer **II**		Approximate
ν	ν	I^{IR}	ν	I^{IR}	Description [b]
b	3208	555	3209	560	νOH
3068	3132	8	3132	8	ν$CH\ r_1$
3040	3109	19	3109	19	ν$CH\ r_1$
3032	3100	4	3101	4	ν$CH\ r_2$
	3094	9	3094	8	ν$CH\ r_1$
2994	3051	34	3068	18	νCH_3 *as* et
	3043	23	3043	3	νCH_3 *as*
	3037	25	3043	28	νCH_3 *as* et
	3035	10	3035	10	νCH_3 *as*
	3026	1	3033	31	νCH_2 *as*
2943	2991	14	3010	23	νCH_2 *s*
	2977	22	2977	23	νCH_3 *s*
	2972	17	2970	18	νCH_3 *s* et
1669/ 1665	1651	337	1650	321	νC=O
1624/ 1616	1611	282	1611	289	ν$CC\ r_2$, δCOH
1607	1606	12	1606	6	ν$CC\ r_1$
1596/ 1583/ 1573	1574	99	1574	97	ν$CC\ r_1,r_2$
1504/ 1498	1496	84	1495	81	ν$CC\ r_1,r_2$
1482	1485	6	1473	23	δCH_2
1468	1465	3	1465	19	δCH_3 *as* et
	1465	17	1459	11	δCH_3 *as*
1458	1453	8	1455	11	δCH_3 *as* et
1451/ 1448	1450	8	1450	8	δCH_3 *as*
1441	1443	31	1442	28	ν$CC\ r_1,r_2$, δ$CH\ r_1$
1427/ 1422	1424	68	1423	72	δCOH
1411	1406	25	1405	20	δ$CH\ r_2$
1406/ 1401	1400	73	1395	85	wCH_2
1396	1392	12	1391	11	δCH_3 *s*
1387/ 1382	1378	154	1377	140	δCH_3 *s* et
	1370	26	1370	24	δCH r1
1357/ 1349	1348	149	1349	162	ν$CC\ r_2$, wCH_2
1330/ 1320	1309	83	1310	76	ν$CC\ r_1,r_2$
1283/ 1277	1271	424	1303	10	ν$CC(=O)$, δ$CH\ r_2$
	1269	1	1271	354	twCH_2
1245	1258	16	1257	12	δ$CH\ r_1$
1229	1221	16	1219	8	ν$CC(H_3)$, ν$CC\ r_2$
1208	1206	287	1204	269	νCN, νC-O
1162	1157	93	1169	43	δ$CH\ r_1$
1151	1149	4	1155	53	γCH_3 et, γCH_2
1136/ 1132	1133	97	1125	124	νCC(=O), νC-O(H)
1117/ 1115/ 1108/ 1099	1107	13	1089	33	γCH_3 et
1085	1083	3	1081	2	ν$CC\ r_1$, γCH_3
1041	1038	2	1038	2	γCH_3
1040	1034	13	1034	13	γCH_3
1031/ 1027/ 1021/ 1010	1013	89	1004	74	νCC et
n.obs.	978	1	979	1	γ$CH\ r_1$
977/ 974	968	22	965	21	ν$CC\ r_1$, γCH_3
950/ 949	941	7	943	7	γ$CH\ r_2$
932	923	17	909	16	δr_1,r_2
899	896	0.3	897	0.3	γ$CH\ r_1$
869	858	2	849	1	νOC et
842/ 839	825	108	828	105	τOH
823	814	32	817	24	δr_2
813/ 810	806	12	807	15	γ$CH\ r_1$
807	796	0.4	803	5	δr_2
804	795	5	782	16	γCH_2
789	780	14	761	5	γ$CH\ r_1$
769	754	12	754	12	ν$CC(=O)$
676	670	0.1	670	0.2	δr_1,r_2
	666	1	667	1	τr_1
613	621	1	622	1	τr_1
595	604	2	601	3	δr_2
575	563	0.4	564	0.1	δr_2
526	522	2	521	2	δr_1
n.obs.	489	0.1	490	0.2	τr_1
489	484	2	483	3	w$C(CH_3)$

DOI: 10.1021/acs.joc.5b02169
J. Org. Chem. XXXX, XXX, XXX−XXX

Table 3. continued

Observed (Ar matrix; 15 K)	Conformer **I**		Conformer **II**		Approximate
ν	ν	I^{IR}	ν	I^{IR}	Description [b]
n.i.	472	1	476	1	tr_1,r_2
	453	2	458	12	wC(C=O)O)
	401	34	404	4	δCC=O
	360	1	387	30	δCCO
	334	1	356	0.1	δCCC et
	283	7	307	5	γC=O, τCH_3 et
	277	6	271	4	δCOC
	255	3	255	3	$\tau r_1,r_2$ (butterfly)
	247	0.3	249	0.4	τCH_3 et
	223	1	225	1	τCH_3
	213	2	220	2	δOCC et
	192	0.04	190	0.03	$\tau r_1,r_2$
	119	1	136	2	τC-O
	113	0.1	113	0.1	τC-O et
	93	1	95	0.1	δCOC, δOCC et
	71	0.2	73	0.2	τr_2
	57	2	43	0.2	γC(C(=O)O)
	16	0.4	41	2	τO-C et

[a]Wavenumbers (ν) in cm^{-1}; IR intensities (I^{IR}) in km mol^{-1}. [b]Assignments and approximate descriptions are specific for conformer **I**; *ν*, stretching; *δ*, in-plane-bending; *γ*, out-of-plane rocking; *τ*, torsion; w, wagging; tw, twisting; r_1 and r_2 refers to the benzene and heteroaromatic ring, respectively; et, ethyl group; *s*, symmetric; *as*, antisymmetric; n.obs., non-observed; n.i., not investigated. [b]As it is common when the molecule contains a very strong intramolecular H-bond, the *ν*OH band is very broad and difficult to distinguish from the baseline. Moreover, in the present case the spectral region where it is expected to occur is quite congested due to the presence of the bands due to the CH stretching modes and also those due to the stretching vibration of the co-deposited H−Cl (see Experimental Section). Under these circumstances, we investigated the precise assignment of this vibration.

which, in view of the low barrier for **II** → **I** conformational interconversion, appear as more plausible explanations for the observations.

The proposed assignments for the bands observed in the experimental spectrum (at 15 K) are summarized in Table 3. In this table, the theoretical wavenumbers and IR intensities for both conformers **I** and **II** of **5Me-HQE** are also provided.

It is worth mentioning that no traces of **5Me-OQE** or **5Me-OQHE** tautomers could be found in the experimental IR spectra (see Figure S14), clearly revealing that the species resulting from sublimation of the used hydrochloride salt (**5Me-HQE·HCl**) are solely HCl and **5Me-HQE**, i.e., the tautomeric species of the compound present in the crystalline solid did not convert, upon sublimation, to other tautomer.

Quite interestingly, the infrared spectrum of a matrix resulting from deposition of the material obtained from **5Me-HQE·HCl** after alkaline washing (5Me-OQE, according to the performed ATR experiments) revealed that the **5Me-OQE** keto form undergoes extensive tautomerization to the most stable hydroxyquinoline form (**5Me-HQE**) upon sublimation, since this spectrum is identical to that obtained upon deposition of the unwashed **5Me-HQE·HCl** sample.

In situ broadband UV (*λ* > 220 nm) irradiation of matrix isolated **5Me-HQE** for 130 min led to consumption of about one-third of the original compound. However, the number of new bands detected in the spectra of the photolyzed matrix was very small (Figure 10). These new bands appear at 2343 cm^{-1}, indicating formation of CO_2,[33] in the 2156−2106 cm^{-1} range, and at 1734 cm^{-1}. The bands in the 2156−2106 cm^{-1} range shall be due to both CO and ketene species.[34−37] The photoproduction of ketene species from **5Me-HQE** is supported by the following facts: (i) ketenes are well-known to give rise to a very intense (>900 km mol^{-1}) infrared band in the 2150−2100 cm^{-1} range due to the *ν*C═C═O antisymmetric stretching, which is very sensitive to the specific conformation adopted by the ketene,[37] thus in general

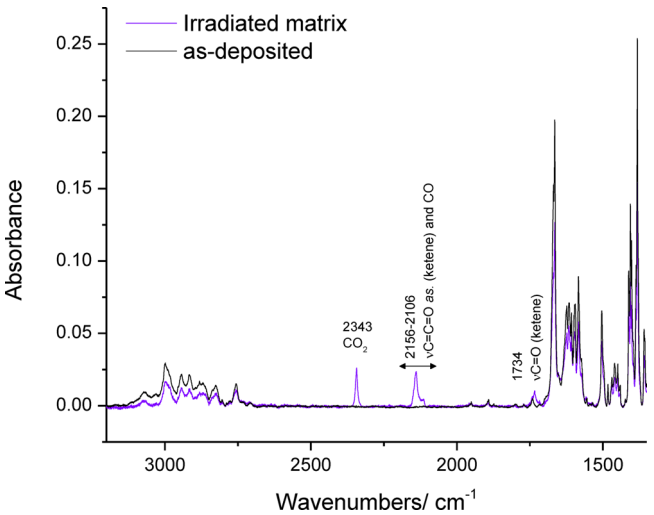

Figure 10. Fragment of the IR spectra showing photolysis (130 min.; *λ* > 220 nm) of **5Me-HQE** in argon matrix. In black: IR spectrum obtained prior to irradiation; and in purple: IR spectrum obtained after irradiation. Bands due to CO, CO_2, and ketene species are identified (see text).

appearing as a band exhibiting several components, as it is observed in the present case; (ii) formation of ketenes has been observed for similar compounds isolated in matrices and subjected to similar irradiation conditions, for example, methyl *p*-hydroxybenzoic acid (methyl paraben) and triclosan.[38,39] The mechanism for ketene formation involves most probably the initial formation of the **5Me-HQE** phenoxyl radical, as observed for methyl *p*-hydroxybenzoic acid and triclosan[38,39] and for phenol derivatives in general (in the case of phenol and phenol-d_5, the formed radical could be detected and characterized spectroscopically in the cryogenic matrices).[40] Subsequent recombination of the hydrogen radical and ring-opening by

DOI: 10.1021/acs.joc.5b02169
J. Org. Chem. XXXX, XXX, XXX−XXX

cleavage of an α-bond to the OH ring-substituent leads to production of the ketene; (iii) the photoproduced ketene contains a carbonyl bond, whose absorption band in the infrared is also expected to be intense (~200−300 km mol^{-1}).[38] Thus, the new band observed at 1734 cm^{-1} also supports the formation of ketene species upon photolysis of **5Me-HQE** in argon matrix. Note that, besides these two bands, all other bands ascribed to ketenes are expected to be of low intensity and, in most of the cases, to overlap with bands due to the reactant, which explains the non-observation of additional ketene bands in the spectra of the photolyzed matrix. Similarly, no bands were observed, in the spectra of the photolyzed matrix, that could be attributed to the photoproducts of the decarboxylation and decarbonylation reactions of the ester moiety of **5Me-HQE**, accompanying the production of the identified CO_2 and CO.

In summary, the performed photochemical experiments indicate that **5Me-HQE** is relatively photostable. Upon continuous broadband UV (λ > 220 nm) irradiation of the matrix-isolated compound for 130 min, only about one-third of the compound reacted, giving rise to an open-ring ketene isomeric species. Decomposition of the compound was also observed, resulting in CO_2 and CO release.

Biological Activity and cLog *P* Calculations. As pointed out in the Introduction, the knowledge of tautomeric and conformational preferences for compounds **7Me-OQE** (**5**, R = CH_3) and **5Me-HQE** (**10**) is important for predicting and/or explaining biological activity. According to docking studies performed for selected quinolone 3-esters on yeast *bc1*,[14] the 4-oxoquinoline 3-ester form **7Me-OQE** should present a much better pharmacological profile as *P. falciparum* bc_1 inhibitor than its 4-hydroxyquinoline 3-ester isomer **5Me-HQE**, with the N−H and 4-oxo groups of **7Me-OQE** being involved in important interactions inside the enzyme pocket. However, a change in structure will translate in change of chemical and physical properties (like solubility), with possible impact on pharmacologic performance.

We determined the clog *P* values for compounds prepared, **7Me-OQE** and **5Me-HQE**, and for corresponding tautomers, **7Me-HQE** and **5Me-OQE**. The antimalarial activity of **7Me-OQE** and **5Me-HQE** were evaluated against the chloroquine-resistant strain Dd2 of *P. falciparum*. Results are presented in Table 4. As shown in this table, the keto forms (**5** and **11**) have a lower clog *P* than the corresponding hydroxy forms (**6** and **10**). Thus, the keto forms have a higher aqueous solubility, but their reduced lipophilicity decreases the passage through biological membranes. So, the clog *P* values exhibited by the hydroxy forms appear more adequate from a bioavailability viewpoint, although their pharmacodynamic profile as inhibitors of the *P. falciparum* bc_1 complex is expected to be less favorable, in view of the results from docking studies.

Table 4. cLog *P* for 7Me-OQE (5), 7Me-HQE (6), 5Me-HQE (10), and 5Me-OQE (11) and in Vitro Antimalarial Activities of 5 and 10

	7Me-OQE (5)	7Me-HQE (6)	5Me-HQE (10)	5Me-OQE (11)
clog P^a ± SD	1.90 ± 0.40	2.88 ± 0.51	2.87 ± 0.51	1.99 ± 0.31
IC_{50} (μM) Dd2 ± SD	3.03 ± 0.35	n.d.	5.89 ± 1.54	n.d.

[a]By ALog PS2.1.

5-Methyl-4-hydroxyquinoline 3-ester, **5Me-HQE**, exhibited activity against *P. falciparum* Dd2 at micromolar concentrations (IC_{50} of 5.89 μM). The oxo-tautomer, 5-methyl-4-oxoquinoline 3-ester, **5Me-OQE**, is energetically less stable than **5Me-HQE** by more than 20 kJ mol^{-1} in the gas phase and was not detected in solution (DMSO) or in the condensed phase (except in the material resulting from alkaline washing of the hydrochloride salt of the compound). It was not evaluated against *P. falciparum* Dd2. However, from the viewpoint of keto−enol tautomerism, **5Me-HQE** may be compared to **7Me-OQE**, prepared by thermal cyclization in Dowtherm A (Scheme 1; route c). The difference between **5Me-OQE** and **7Me-OQE** resides solely on the position of the methyl substituent, which should not affect the keto−enol equilibrium. 4-Oxoquinoline **7Me-OQE** was evaluated against *P. falciparum* Dd2 showing antiplasmodial activity only slightly higher than **5Me-HQE** (IC_{50} of 3.03 μM). These results may look somewhat surprising if we consider published results from docking studies, since the 4-hydroxy and 4-oxo tautomers exhibit similar activity. However, it is worth considering the lower value of clog *P* for **7Me-OQE**, compared to **5Me-HQE**, so the better pharmacodynamic performance may be offset by the poor bioavailability. This is in keeping with the proposal of optimizing 7-substituted quinolone 3-esters **5** by tailoring the substituent in position 7. On the other hand, understanding the micromolar activity of **5Me-HQE** requires further investigations. The 4-hydroxyquinoline 3-ester chemotype may bind differently to the same pocket or may even switch to the Q_i site of the bc_1 complex. Such a change in the primary target for the quinolone ester class might enhance activity versus atovaquone-resistant strains. Docking studies should be undertaken with this class, using relevant enzyme targets.

CONCLUSIONS

In recent years, quinolone 3-esters were investigated as inhibitors targeting the Q_o site of the bc_1 protein complex of *P. falciparum*. Docking studies performed in silico at the yeast Q_o site suggested a key role for residues His182 and Glu272 (in the target ISP) in the recognition of high potency inhibitors and established that the 4-oxo and N−H groups appear to be important to the inhibitory activity of quinolone 3-esters toward *P. falciparum* bc_1 protein complex.[14]

Although some 7-substituted quinolone 3-esters appear highly promising as drug leads, with activity against both the enzyme and the parasite at low nanomolar concentrations, the compounds present liabilities, such as poor aqueous solubility and low oral bioavailability. Preliminary results from SAR studies indicated that optimization could be achieved by tuning the nature of substituent at position 7.[14] However, considering that the information from docking studies in silico establishes a key role for 4-oxo and the N−H groups in drug-target interactions, the possibility of tautomerism between 4-oxoquinoline and 4-hydroxyquinoline forms (**5**, **6**; Figure 2) should not be neglected. Tautomerization will translate in alteration of chemical and physical properties, with consequences for pharmacokinetic and pharmacodynamic profiles and should therefore be investigated.

We describe the synthesis and structure of **7Me-OQE** and **5Me-HQE**. **7Me-OQE** was obtained from **9** by thermal cyclization in Dowtherm A at 250 °C (see Scheme 1, route c) and isolated as sole product. **5Me-HQE** was also obtained as sole product from compound **9**, by conducting the reaction in the presence of $POCl_3$, at 100 °C. The crystal structures of

DOI: 10.1021/acs.joc.5b02169
J. Org. Chem. XXXX, XXX, XXX−XXX

malonate derivative **9** and **5Me-HQE** were investigated by X-ray crystallography.

5Me-HQE and **7Me-OQE** were theoretically investigated (B3LYP/6-311++G(d,p)). A detailed analysis of conformational and tautomeric preferences is provided, and the possibility of quinolone-hydroxyquinoline equilibria is evaluated. Calculations show preference for the hydroxyquinoline form in both compounds. The difference between the lowest energy hydroxyquinoline and quinolone forms is 27 and 38 kJ mol^{-1} for **5Me-HQE** and **7Me-OQE**, respectively. The considerably lower energy of hydroxyquinoline forms can be correlated with the presence in these forms of a O−H···$O_{(carbonyl)}$ stabilizing intramolecular H-bond interaction.

HOMA and B_I aromaticity indexes were determined for **5Me-HQE** and its **5Me-OQE** and **5Me-OQHE** tautomers, using the B3LYP/6-311++G(d,p) calculated bond lengths. Qualitatively, the two indexes agree with each other. While in **5Me-HQE** both rings are aromatic, with the heteroaromatic ring being only slightly less aromatic than the benzenic ring, in both **5Me-OQE** and **5Me-OQHE** the nitrogen-containing ring is essentially non-aromatic; the benzenic ring being in these cases somewhat more aromatic than in **5Me-HQE**. The reduced aromaticity of the heterocyclic ring in both **5Me-OQE** and **5Me-OQHE** compared to **5Me-HQE** can then also be considered a relevant factor, rendering these species more energetic than **5Me-HQE**.

The structure of monomeric **5Me-HQE** was also studied using matrix isolation coupled to FTIR spectroscopy. No traces of **5Me-OQE** or **5Me-OQHE** tautomers were found in the experimental matrix isolation IR spectra, clearly revealing that the species resulting from sublimation of the used hydrochloride salt (**5Me-HQE·HCl**) are solely HCl and **5Me-HQE**, i.e., the tautomeric species of the compound present in the crystalline solid did not convert to other tautomer, upon sublimation. On the contrary, when solid **5Me-OQE** was used as starting material in the matrix isolation experiments, extensive tautomerization of the compound was observed, resulting in the sole observation of the quinoline tautomeric form, **5Me-HQE**.

Upon continuous broadband UV (λ > 220 nm) irradiation of the matrix-isolated **5Me-HQE** for 130 min, only about one-third of the compound reacted, giving rise to an open-ring ketene isomeric species. Decomposition of the compound was also observed, resulting in CO_2 and CO release. Thus, **5Me-HQE** appears to be relatively photostable.

The antiplasmodial activity of 4-oxoquinoline **7Me-OQE** and 4-hydroxyquinoline **5Me-HQE** against chloroquine and mefloquine-resistant *P. falciparum* strain Dd2[22] was evaluated. Both compounds exhibited activity at low micromolar concentrations with IC_{50} values of 3.03 μM for **7Me-OQE** and 5.89 μM for **5Me-HQE**. The 4-oxoquinoline is only slightly more active than the 4-hydroxyquinoline. Given the low clog *P* value for **7Me-OQE** compared to **5Me-HQE**, a better pharmacodynamic performance may be offset by the poor bioavailability.

Our results support the proposal of optimizing 7-substituted 4-oxoquinoline 3-esters **5** by tailoring the substituent in position 7 and also expose the relevance of exploring 4-hydroquinoline 3-esters as scaffolds. The 4-hydroxyquinoline 3-ester chemotype may bind differently to the same pocket or may even switch to the Q_i site of the bc_1 complex. Such a change in the primary target for the quinolone ester class might enhance activity versus atovaquone-resistant strains. Docking studies should be undertaken with this class, using relevant enzyme targets.

EXPERIMENTAL SECTION

General Methods. All reagents and solvents were purchased from commercial sources and used as received. When required, solvents were freshly distilled from appropriate drying agents before use. The reactions were monitored by TLC, using silica gel F254 plates. Purifications by flash column chromatography were performed with 40−63 mesh silica gel. When required, inorganic solids were removed by filtration through a layer of Celite 512 medium. NMR (400 MHz) spectra for compounds, in appropriate solvents (d_6-DMSO or *d*-chloroform), were measured using TMS as the internal reference (δ = 0.0 ppm). Chemical shifts (δ) are described in parts per million (ppm). Splitting patterns are designated as s (singlet), d (doublet), t (triplet), q (quartet), and m (multiplet). NMR spectra for target compounds, operated at 400 and 100 MHz, for ^{1}H and ^{13}C, respectively, are provided in Figures S2, S3, and S5−S9. Melting points were recorded and are uncorrected.

Preparation of 3-Methylaniline (*m*-Toluidine) (8). 3-Nitrotoluene (**7**) (4 mL; 33.75 mmol) was dissolved in a mixture of methanol and water (1:1; 60 mL). Ammonium chloride (6.7 equiv) was added, followed by iron powder (4.2 equiv), and the resulting mixture was stirred vigorously at 60 °C for 4 h. The reaction mixture was cooled, then diluted with methanol, and filtered through Celite. The filtrate was concentrated by evaporation under reduced pressure, and the aqueous residue was extracted with EtOAc. The combined organic extracts were dried over $MgSO_4$, filtered, and evaporated to dryness. 3-Methylaniline (**8**) was recovered as brown oil (3.4 g; 94% yield). ^{1}H NMR (400 MHz, $(CD_3)_2SO$) δ 6.88 (t, *J* = 7.6 Hz, 1H), 6.34 (m, 3H), 4.88 (s, 2H), 2.14 (s, 3H). ^{13}C NMR (100 MHz, $CDCl_3$) δ 147.4, 139.1, 130.2, 119.4, 115.8, 113.0, 22.3. MS *m*/*z* (GC-TOF, EI+): 107.1490 ($[M]^+$). These results are compatible with those described in the literature about this compound.[41]

Preparation of Diethyl 2-[((3-Methylphenyl)amino)-methylene]malonate (9). 3-Methylaniline (**8**) (3 mL; 28 mmol) and diethyl ethoxymethylenemalonate (5.7 mL; 28 mmol) were stirred at 100 °C, overnight. Purification by column chromatography (eluting with DCM) followed by recrystallization in ethanol and DCM yielded diethyl 2-[((3-methylphenyl)amino)methylene]malonate (**9**) as a creamy crystal (7.1 g; 92%). Melting range 38−39 °C. ^{1}H NMR (400 MHz, $(CD_3)_2SO$) δ 10.63 (d, 1H), 8.40 (s, 1H), 7.25 (t, *J* = 7.1 Hz, 1H), 7.18−7.06 (m, 2H), 6.96 (s, 1H), 4.14 (m, 4H), 2.29 (s, 3H), 1.23 (m, 6H). ^{13}C NMR (101 MHz, $(CD_3)_2SO$) δ 168.0, 165.4, 151.5, 139.7, 139.6, 129.9, 125.8, 118.3, 115.0, 93.4, 60.1, 59.9, 23.4, 14.7, 14.6. MS *m*/*z* (GC-TOF, EI+): 277.1312 ($[M]^+$), 231.0901 ($[M - OEt]^+$), 203.0962 ($[M - CO_2Et]^+$), 186.0569 ($[M - 2xOEt]^+$), 158.0745 ($[M - CO_2Et$ and $OEt]^+$), 130.0682 ($[M - 2xCO_2Et]^+$). CHNS for $C_{15}H_{19}NO_4$ (**9**) requires: C 64.97, H 6.91, N 5.05; found: C 65.07, H 6.95, N 4.77.

Preparation of 7Me-OQE (5, R = CH_3). Diethyl 2-[((3-methylphenyl)amino)methylene]malonate (**9**) (1.07 g; 3.9 mmol) was suspended in Dowtherm A (10 mL), under a nitrogen atmosphere, and the mixture was heated at 250 °C for 3 h. The reaction mixture was cooled to room temperature. The solid precipitate was filtered, washed with hexane and diethyl ether, and dried to afford ethyl 4-oxo-7-methylquinoline-3-carboxylate (**5**) as white powder (0.11 g; 12%). Melting range 282−284 °C. ^{1}H NMR (400 MHz, $(CD_3)_2SO$) δ 12.17 (s, 1H), 8.49 (s, 1H), 8.04 (d, *J* = 8.2 Hz, 1H), 7.38 (s, 1H), 7.24 (d, *J* = 8.2 Hz, 1H), 4.25−4.17 (m, 2H), 2.44 (s, 3H), 1.28 (t, *J* = 7.1 Hz, 3H). ^{1}H NMR (400 MHz, $CDCl_3$) δ 12.20 (s, 1H), 8.52 (s, 1H), 8.26 (d, *J* = 8.1 Hz, 1H), 7.38 (s, 1H), 7.25 (d, *J* = 8.2 Hz, 1H), 4.35 (2H), 2.48 (s, 3H), 1.39 (3H). ^{13}C NMR (101 MHz, $(CD_3)_2SO$) δ 176.0, 165.0, 143.5, 140.6, 140.0, 131.6, 127.4, 125.3, 117.0, 111.0, 59.6, 23.4, 14.4. HRMS (CI) for $C_{13}H_{14}NO_3$ ($[M + H]^+$) requires 232.0974; found 232.0977. CHNS for $C_{13}H_{13}NO_3$ (**5**, R = CH_3) requires: C 67.53, H 5.67, N 6.06; found: C 67.29, H 5.63, N 5.96.

DOI: 10.1021/acs.joc.5b02169
J. Org. Chem. XXXX, XXX, XXX−XXX

Preparation of 5Me-HQE (10). Diethyl 2-[((3-methylphenyl)-amino)methylene]malonate (**9**) (1.37 g; 5 mmol) was suspended in phosphoryl chloride (15 mL), under a nitrogen atmosphere, and the resulting mixture was refluxed overnight at 97 °C. The excess of phosphoryl chloride was evaporated under reduced pressure. The resulting residue was cooled to 90 °C and diluted with isopropanol. The mixture was left to cool slowly, while a solid precipitate was formed. After filtration, washing with cold isopropanol and then with cold light petroleum ether, a mixture of a powder and orange crystals was recovered. The crystalline product was identified as ethyl 4-hydroxy-5-methylquinolinium chloride 3-carboxylate (0.25 g; 22% yield), as confirmed by X-ray crystallography. Melting range 146−147 °C. ^{1}H NMR (400 MHz, $(CD_3)_2SO$) δ 8.38 (s, 1H), 7.49 (t, J = 7.1 Hz, 1H), 7.44 (d, J = 8.2 Hz, 1H), 7.10 (d, J = 8.2 Hz, 1H), 4.18 (q, 2H), 2.78 (s, 3H), 1.26 (t, 3H). ^{1}H NMR (400 MHz, $CDCl_3$) δ 9.26 (s, 1H), 8.51 (d, 1H), 7.91 (t, 1H), 7.59 (d, 1H), 4.58 (q, 2H), 3.01 (s, 3H), 1.50 (t, 3H). ^{13}C NMR (101 MHz, $(CD_3)_2SO$) δ 171.1, 171.1, 161.3, 144.6, 144.1, 140.1, 140.6, 132.0, 127.9, 117.3, 114.3, 60.1, 23.9, 14.8. MS m/z (GC-TOF, EI+): 231.0899 ($[M]^+$). NMR and MS data are compatible with **5Me-HQE** (compound **10**). The powder was submitted to elemental analysis. CHNS for $C_{13}H_{13}NO_3$ (**10**) requires: C 67.53, H 5.67, N 6.06; found: C 67.43, H 5.63, N 6.03.

The crystalline **5Me-HQE·HCl** washed with aqueous sodium bicarbonate and the remaining mixture was extracted with chloroform. The organic layer was evaporated to dryness to afford an amorphous powder that was characterized by ATR-IR and proved to be the keto form, **5Me-OQE**, showing conversion of the 4-hydroxyquinoline form to the 4-oxoxyquinoline tautomer in basic media.

Computational Methods. All theoretical calculations were performed using Gaussian 09,[42] at the DFT(B3LYP)/6-311++G(d,p) level of theory.[43−46] Calculated harmonic vibrational wavenumbers were uniformly scaled by 0.978. The scaled calculated frequencies, together with the calculated intensities, were used to produce the simulated spectra shown in the figures; bands were broadened by Lorentzian function, with a full-width-at-half-maximum of 2 cm^{-1}. The potential energy profiles for internal rotation were calculated with the driving coordinate incrementally fixed and all the other geometrical parameters optimized.

Matrix Preparation, Infrared Spectroscopy, and Irradiation Experiments. Matrices were prepared by heating a solid sample of the hydrochloride salt of **5Me-HQE** or of **5Me-OQE** (resulting from the alkaline washing of the hydrochloride **5Me-HQE** salt) in a miniature thermoelectrically heatable glass furnace placed in the vacuum chamber of the cryostat (APD Cryogenics closed-cycle helium refrigerator with a DE-202A expander). Upon sublimation, the salt released HCl, as testified by observation of the characteristic bands of HCl isolated in an argon matrix at 2888, 2869, and 2854 cm^{-1} (monomer), 2856, 2818 cm^{-1} (dimer), 2787 cm^{-1} (trimer), and 2748 cm^{-1} (tetramer).[47,44] Together with HCl, **5Me-HQE** vapor was formed, being codeposited with a large excess of argon (N60; supplied by commercial supplier) onto the CsI substrate of the cryostat, kept at 17 K during deposition of the matrix. When the **5Me-OQE** solid sample was used to prepare the low temperature matrices, the obtained argon matrices were shown to contain only the hydroxyquinoline tautomeric form of the compound, testifying the occurrence of the quinolone → quinoline tautomerization upon sublimation.

The IR spectra were recorded in the range 4000−400 cm^{-1}, with a resolution of 0.5 cm^{-1}, using a Thermo Nicolet 6700 Fourier-transform infrared (FTIR) spectrometer, equipped with a KBr beam splitter and a deuterated triglycine sulfate (DTGS) detector. UV irradiation of the matrices was done through the outer quartz window of the cryostat, using a HBO200 high-pressure Hg(Xe) lamp.

ATR- FTIR Experiments. The ATR-FTIR spectra were obtained using a germanium crystal in a Nicolet iN10 MX infrared system with a MCT-A detector and a KBr/Germanium optics. The spectral resolution used was 2 cm^{-1}, with aperture and number of scans of 80 and 64, respectively.

Crystallographic Analysis. X-ray data were collected using small single crystals of the compounds in study. The crystallographic structures were solved by direct methods using SHELXT-2014/4.[48] Refinements were carried out with the SHELXL-2014/7 package.[49] All refinements were made by full-matrix least-squares on F^2 with anisotropic displacement parameters for all non-hydrogen atoms see tables in Sections A and B in the Supporting Information for details regarding crystallographic analysis of compound **9** and of **5Me-HQE·HCl**. In the latter compound the ethyl group is disordered over two positions with relative occupancies of 70:30%. Appropriate SADI and ISOR restraints were applied to the C atoms of this group. All of the hydrogen atoms (except for those of the disordered part) could be located on a difference Fourier synthesis; their positions were refined as riding on parent atoms with an isotropic temperature factor using SHELXL-2014/7 defaults that constrain these atoms to idealized positions, except for the coordinates of the H atom of the amino group of compound **9**, involved in strong H-bonding, were freely refined. The X-ray analysis unambiguously demonstrate the presence of diethyl 2-[((3-methylphenyl)amino)methylene]malonate (**9**) and **5Me-HQE·HCl**, respectively (see Figures S4 and S11, and Sections A and B in Supporting Information).

In Vitro Antimalarial Activity and clog *P* Calculations. Laboratory-adapted chloroquine and mefloquine-resistant *P. falciparum* Dd2[22] was continuously cultured as previously described by Trager and Jensen[50] and synchronized by sorbitol treatment prior to the assays.[51] Staging and parasitaemia were determined by light microscopy of Giemsa-stained thin blood smears. Antimalarial activity of the compounds was determined using the SYBR Green I assay as previously described,[49,50] with modifications. Briefly, early ring stage parasites (>90% of rings, 3% hematocrit and 1% parasitaemia) were tested in triplicate in a 96-well plate and incubated with the compounds for 48h (37 °C, 5% CO_2), parasite growth was assessed with SYBR Green I. Each compound was tested in concentrations ranging from 10 to 0.002 μM. Fluorescence intensity was measured with a multimode microplate reader (Dynex Triad, Alfagene) with excitation and emission wavelengths of 485 and 535 nm, respectively, and analyzed by nonlinear regression using GraphPad Prism 5 demo version to determine IC_{50}. cLog *P* calculations were performed using ALog PS2.1, as shown in http://www.vcclab.org/lab/alogps/.

■ ASSOCIATED CONTENT

Supporting Information

The Supporting Information is available free of charge on the ACS Publications website at DOI: 10.1021/acs.joc.5b02169.

Representative quinolones as antibacterial agents; ^{1}H and/or ^{13}C NMR spectra of **8**, **9**, **7Me-OQE**, and **5Me-HQE**; ATR-IR spectra and table of observed ATR-IR frequencies for **5Me-HQE** and **7Me-OQE** crystals; calculated infrared spectra of its two lower energy conformers; table of experimental (X-ray, single-crystal) details of the crystallographic studies; ORTEPII plot of the compound 9 and **5Me-HQE·HCl** (PDF)

Crystallographic data for **5Me-HQE·HCl** (CIF)

Crystallographic data for **9** (CIF)

■ AUTHOR INFORMATION

Corresponding Authors

*E-mail: rfausto@ci.uc.pt.

*E-mail: mcristi@ualg.pt.

Notes

The authors declare no competing financial interest.

■ ACKNOWLEDGMENTS

The authors gratefully acknowledge Fundação para a Ciência e a Tecnologia (FCT), Portugal (Project PEst-C/MAR/LA0015/603 2013), cofounded by QREN-COMPETE-UE and CCMAR for generous financial support. The Coimbra Chemistry Centre

DOI: 10.1021/acs.joc.5b02169
J. Org. Chem. XXXX, XXX, XXX−XXX

(CQC) is also supported by FCT through Project PEst-OE/QUI/UI0313/2014. P.H. acknowledges FCT for the award of a doctoral grant (SFRH/BD/81821/2011). N.K acknowledges FCT for the award of a postdoctoral grant (SFRH/BPD/88372/2012). NMR spectrometers used are part of The National NMR Facility, supported by Fundação para a Ciência e a Tecnologia (RECI/BBB-BQB/0230/2012).

REFERENCES

(1) Sissi, C.; Palumbo, M. *Curr. Med. Chem.: Anti-Cancer Agents* **2003**, *3*, 439−450.
(2) Kim, O. K.; Ohemeng, K.; Barrett, J. F. *Expert Opin. Invest. Drugs* **2001**, *10*, 199−212.
(3) Boteva, A. A.; Krasnykh, O. P. *Chem. Heterocycl. Compd.* **2009**, *45*, 757−785.
(4) Nakamura, S.; Kozuka, M.; Bastow, K. F.; Tokuda, H.; Nishino, H.; Suzuki, M.; Tatsuzaki, J.; Morris Natschke, S. L.; Kuo, S.-C.; Lee, K.-H. *Bioorg. Med. Chem.* **2005**, *13*, 4396−4401.
(5) Tedesco, R.; Shaw, A. N.; Bambal, R.; Chai, D.; Concha, N. O.; Darcy, M. G.; Dhanak, D.; Fitch, D. M.; Gates, A.; Gerhardt, W. G.; Halegoua, D. L.; Han, C.; Hofmann, G. A.; Johnston, V. K.; Kaura, A. C.; Liu, N.; Keenan, R. M.; Lin-Goerke, J.; Sarisky, R. T.; Wiggall, K. J.; Zimmerman, M. N.; Duffy, K. J. *J. Med. Chem.* **2006**, *49*, 971−983.
(6) Kumar, D. V.; Rai, R.; Brameld, K. A.; Somoza, J. R.; Rajagopalan, R.; Janc, J. W.; Xia, Y. M.; Ton, T. L.; Shaghafi, M. B.; Hu, H.; Lehoux, I.; To, N.; Young, W. B.; Green, M. J. *Bioorg. Med. Chem. Lett.* **2011**, *21*, 82−87.
(7) Serrao, E.; Debnath, B.; Otake, H.; Kuang, Y.; Christ, F.; Debyser, Z.; Neamati, N. *J. Med. Chem.* **2013**, *56*, 2311−2322.
(8) Dorow, R. L.; Herrinton, P. M.; Hohler, R. A.; Maloney, M. T.; Mauragis, M. A.; McGhee, W. E.; Moeslein, J. A.; Strohbach, J. W.; Veley, M. F. *Org. Process Res. Dev.* **2006**, *10*, 493−499.
(9) Sultana, N.; Naz, A.; Khan, B.; Arayne, M. S.; Mesaik, M. A. *Med. Chem. Res.* **2010**, *19*, 1210−1221.
(10) Kathrotiya, H. G.; Patel, M. P. *Eur. J. Med. Chem.* **2013**, *63*, 675−684.
(11) Pidathala, C.; Amewu, R.; Pacorel, B.; Nixon, G. L.; Gibbons, P.; Hong, W. D.; Leung, S. C.; Berry, N. G.; Sharma, R.; Stocks, P. A.; Srivastava, A.; Shone, A. E.; Charoensutthivarakul, S.; Taylor, L.; Berger, O.; Mbekeani, A.; Hill, A.; Fisher, N. E.; Warman, A. J.; Biagini, G. A.; Ward, S. A.; O'Neill, P. M. *J. Med. Chem.* **2012**, *55*, 1831−1843.
(12) Leung, S. C.; Gibbons, P.; Amewu, R.; Nixon, G. L.; Pidathala, C.; Hong, W. D.; Pacorel, B.; Berry, N. G.; Sharma, R.; Stocks, P. A.; Srivastava, A.; Shone, A. E.; Charoensutthivarakul, S.; Taylor, L.; Berger, O.; Mbekeani, A.; Hill, A.; Fisher, N. E.; Warman, A. J.; Biagini, G. A.; Ward, S. A.; O'Neill, P. M. *J. Med. Chem.* **2012**, *55*, 1844−1857.
(13) Biagini, G. A.; Fisher, N.; Shone, A. E.; Mubaraki, M. A.; Srivastava, A.; Hill, A.; Antoine, T.; Warman, A. J.; Davies, J.; Pidathala, C.; Amewu, R. K.; Leung, S. C.; Sharma, R.; Gibbons, P.; Hong, D. W.; Pacorel, B.; Lawrenson, A. S.; Charoensutthivarakul, S.; Taylor, L.; Berger, O.; Mbekeani, A.; Stocks, P. A.; Nixon, G. L.; Chadwick, J.; Hemingway, J.; Delves, M. J.; Sinden, R. E.; Zeeman, A.-M.; Kocken, C. H. M.; Berry, N. G.; O'Neill, P. M.; Ward, S. A. *Proc. Natl. Acad. Sci. U. S. A.* **2012**, *109*, 8298−8303.
(14) Cowley, R.; Leung, S.; Fisher, N.; Al-Helal, M.; Berry, N. G.; Lawrenson, A. S.; Sharma, R.; Shone, A. E.; Ward, S. A.; Biagini, G. A.; O'Neill, P. M. *MedChemComm* **2012**, *3*, 39−44.
(15) *World Malaria Report 2014*; World Health Organization: Geneva, Switzerland, 2014.
(16) Biagini, G. A.; Viriyavejakul, P.; O'neill, P. M.; Bray, P. G.; Ward, S. A. *Antimicrob. Agents Chemother.* **2006**, *50*, 1841−1851.
(17) Hammond, D. J.; Burchell, J. R.; Pudney, M. *Mol. Biochem. Parasitol.* **1985**, *14*, 97−109.
(18) Stephen, J. M. L.; Tonkin, I. M.; Walker, J. *J. Chem. Soc.* **1947**, 1034−1039.
(19) Beteck, R. M.; Smit, F. J.; Haynes, R. K.; N'Da, D. D. *Malar. J.* **2014**, *13*, 339.
(20) Nilsen, A.; LaCrue, A. N.; White, K. L.; Forquer, I. P.; Cross, R. M.; Marfurt, J.; Mather, M. W.; Delves, M. J.; Shackleford, D. M.; Saenz, F. E.; Morrisey, J. M.; Steuten, J.; Mutka, T.; Li, Y.; Wirjanata, G.; Ryan, E.; Duffy, S.; Kelly, J. X.; Sebayang, B. F.; Zeeman, A.-M.; Noviyanti, R.; Sinden, R. E.; Kocken, C. H. M.; Price, R. N.; Avery, V. M.; Angulo-Barturen, I.; Jiménez-Díaz, M. B.; Ferrer, S.; Herreros, E.; Sanz, L. M.; Gamo, F.-J.; Bathurst, I.; Burrows, J. N.; Siegl, P.; Guy, R. K.; Winter, R. W.; Vaidya, A. B.; Charman, S. A.; Kyle, D. E.; Manetsch, R.; Riscoe, M. K. *Sci. Transl. Med.* **2013**, *5*, 177ra37.
(21) Puri, S. K.; Dutta, G. P. *Trans. R. Soc. Trop. Med. Hyg.* **1990**, *84*, 759−760.
(22) Oduola, A. M.; Milhous, W.; Weatherly, N.; Bowdre, J.; Desjardins, R. *Exp. Parasitol.* **1988**, *67*, 354−360.
(23) Gould, R. G.; Jacobs, W. A. *J. Am. Chem. Soc.* **1939**, *61*, 2890−2895.
(24) Willard, A. K.; Smith, R. L.; Cragoe, E. J. *J. Org. Chem.* **1981**, *46*, 3846−3852.
(25) Horta, P. C.; Henriques, M. S. C.; Kuş, N.; Paixão, J. a.; O'Neill, P. M.; Cristiano, M. L. S.; Fausto, R. *Tetrahedron* **2015**, *71*, 7583−7592.
(26) Smith, M. B.; March, J.*March's Advanced Organic Chemistry: Reactions, Mechanisms, and Structure*; John Wiley & Sons, Inc.: Hoboken, NJ, 2007.
(27) Teixeira-Dias, J. J. C.; Fausto, R.; de Carvalho, L. A. E. B. *J. Comput. Chem.* **1991**, *12*, 1047−1057.
(28) Fausto, R.; de Carvalho, L. A. E. B.; Teixeira-Dias, J. J. C.; Ramos, M. N. *J. Chem. Soc., Faraday Trans. 2* **1989**, *85*, 1945.
(29) Kruszewski, J.; Krygowski, T. M. *Tetrahedron Lett.* **1972**, *13*, 3839−3842.
(30) Krygowski, T. M. *J. Chem. Inf. Model.* **1993**, *33*, 70−78.
(31) Bird, C. W. *Tetrahedron* **1985**, *41*, 1409−1414.
(32) Reva, I. D.; Lopes Jesus, A. J.; Rosado, M. T. S.; Fausto, R.; Ermelinda Eusébio, M.; Redinha, J. S. *Phys. Chem. Chem. Phys.* **2006**, *8*, 5339.
(33) Lakhlifi, A.; Chabbi, H.; Dahoo, P. R.; Teffo, J. L. *Eur. Phys. J. D* **2000**, *12*, 435−448.
(34) Dubost, H.; Abouaf-Marguin, L. *Chem. Phys. Lett.* **1972**, *17*, 269−273.
(35) Raducu, V.; Gauthier-Roy, B.; Dahoo, R.; Abouaf-Marguin, L.; Langlet, J.; Caillet, J.; Allavena, M. *J. Chem. Phys.* **1996**, *105*, 10092.
(36) Kuş, N.; Breda, S.; Reva, I.; Tasal, E.; Ogretir, C.; Fausto, R. *Photochem. Photobiol.* **2007**, *83*, 1237−1253.
(37) Breda, S.; Reva, I.; Lapinski, L.; Fausto, R. *Phys. Chem. Chem. Phys.* **2004**, *6*, 929.
(38) Kuş, N.; Bayarı, S. H.; Fausto, R. *J. Phys. Chem. B* **2013**, *117*, 13543−13555.
(39) Kuş, N.; Reva, I.; Bayarı, S.; Fausto, R. *J. Mol. Struct.* **2012**, *1007*, 88−94.
(40) Lapinski, L.; Reva, I.; Rostkowska, H.; Halasa, A.; Fausto, R.; Nowak, M. J. *J. Phys. Chem. A* **2013**, *117*, 5251−5259.
(41) Lide, D. R.; Milne, G. W. A. *Handbook of Data on Common Organic Compounds*, 3rd ed.; CRC Press, Inc.: Boca Raton, FL, 1994; Vol *1*.
(42) Frisch, M. J.; Trucks, G. W.; Schlegel, H. B.; Scuseria, G. E.; Robb, M. A.; Cheeseman, J. R.; Scalmani, G.; Barone, V.; Mennucci, B.; Petersson, G. A.; Nakatsuji, H.; Caricato, M.; Li, X.; Hratchian, H. P.; Izmaylov, A. F.; Bloino, J.; Zheng, G.; Sonnenberg, J. L.; Hada, M.; Ehara, M.; Toyota, K.; Fukuda, R.; Hasegawa, J.; Ishida, M.; Nakajima, T.; Honda, Y.; Kitao, O.; Nakai, H.; Vreven, T.; Montgomery, J. A., Jr.; Peralta, J. E.; Ogliaro, F.; Bearpark, M.; Heyd, J. J.; Brothers, E.; Kudin, K. N.; Staroverov, V. N.; Kobayashi, R.; Normand, J.; Raghavachari, K.; Rendell, A.; Burant, J. C.; Iyengar, S. S.; Tomasi, J.; Cossi, M.; Rega, N.; Millam, J. M.; Klene, M.; Knox, J. E.; Cross, J. B.; Bakken, V.; Adamo, C.; Jaramillo, J.; Gomperts, R.; Stratmann, R. E.; Yazyev, O.; Austin, A. J.; Cammi, R.; Pomelli, C.; Ochterski, J. W.; Martin, R. L.; Morokuma, K.; Zakrzewski, V. G.; Voth, G. A.; Salvador, P.; Dannenberg, J. J.; Dapprich, S.; Daniels, A. D.; Farkas, O.; Foresman, J. B.; Ortiz, J. V.; Cioslowski, J.; Fox, D. J. *Gaussian 09*, Revision A.02; Gaussian, Inc.: Wallingford, CT, 2009.

DOI: 10.1021/acs.joc.5b02169
J. Org. Chem. XXXX, XXX, XXX−XXX

(43) McLean, A. D.; Chandler, G. S. *J. Chem. Phys.* **1980**, *72*, 5639.
(44) Becke, A. D. *Phys. Rev. A: At., Mol., Opt. Phys.* **1988**, *38*, 3098−3100.
(45) Lee, C.; Yang, W.; Parr, R. G. *Phys. Rev. B: Condens. Matter Mater. Phys.* **1988**, *37*, 785−789.
(46) Vosko, S. H.; Wilk, L.; Nusair, M. *Can. J. Phys.* **1980**, *58*, 1200−1211.
(47) Maillard, D.; Schriver, A.; Perchard, J. P.; Girardet, C. *J. Chem. Phys.* **1979**, *71*, 517.
(48) Sheldrick, G. M. *Acta Crystallogr., Sect. A: Found. Adv.* **2015**, *71*, 3−8.
(49) Sheldrick, G. M. *Acta Crystallogr., Sect. C: Struct. Chem.* **2015**, *71*, 3−8.
(50) Trager, W.; Jensen, J. B. *J. Parasitol.* **2005**, *91*, 484−486.
(51) Lambros, C.; Vanderberg, J. P. *J. Parasitol.* **1979**, *65*, 418−420.
(52) Carrasco, M. P.; Newton, A. S.; Gonçalves, L.; Góis, A.; Machado, M.; Gut, J.; Nogueira, F.; Hänscheid, T.; Guedes, R. C.; dos Santos, D. J. V. A.; Rosenthal, P. J.; Moreira, R. *Eur. J. Med. Chem.* **2014**, *80*, 523−534.
(53) Bennett, T. N.; Paguio, M.; Gligorijevic, B.; Seudieu, C.; Kosar, A. D.; Davidson, E.; Roepe, P. D. *Antimicrob. Agents Chemother.* **2004**, *48*, 1807−1810.

DOI: 10.1021/acs.joc.5b02169
J. Org. Chem. XXXX, XXX, XXX−XXX